

Published in final edited form as:

*Astron Astrophys.* ; 646: . doi:10.1051/0004-6361/202040076.

## Discovery of the acetyl cation, CH<sub>3</sub>CO<sup>+</sup>, in space and in the laboratory ★

J. Cernicharo<sup>1</sup>, C. Cabezas<sup>1</sup>, S. Bailleux<sup>2</sup>, L. Margulès<sup>2</sup>, R. Motiyenko<sup>2</sup>, L. Zou<sup>2</sup>, Y. Endo<sup>3</sup>, C. Bermúdez<sup>1</sup>, M. Agúndez<sup>1</sup>, N. Marcelino<sup>1</sup>, B. Lefloch<sup>4</sup>, B. Tercero<sup>5,6</sup>, P. de Vicente<sup>5</sup>

<sup>1</sup>Grupo de Astrofísica Molecular, Instituto de Física Fundamental (IFF-CSIC), C/ Serrano 121, 28006 Madrid, Spain

<sup>2</sup>Univ. Lille, CNRS, UMR 8523 - PhLAM - Physique des Lasers Atomes et Molécules, 59000 Lille, France

<sup>3</sup>Department of Applied Chemistry, Science Building II, National Chiao Tung University, 1001 Ta-Hsueh Rd., Hsinchu 30010, Taiwan

<sup>4</sup>CNRS, IPAG, Univ. Grenoble Alpes, F-38000 Grenoble, France

<sup>5</sup>Observatorio Astronómico Nacional (IGN), C/ Alfonso XII, 3, 28014, Madrid, Spain

<sup>6</sup>Centro de Desarrollos Tecnológicos, Observatorio de Yebes (IGN), 19141 Yebes, Guadalajara, Spain

### Abstract

Using the Yebes 40m and IRAM 30m radiotelescopes, we detected two series of harmonically related lines in space that can be fitted to a symmetric rotor. The lines have been seen towards the cold dense cores TMC-1, L483, L1527, and L1544. High level of theory *ab initio* calculations indicate that the best possible candidate is the acetyl cation, CH<sub>3</sub>CO<sup>+</sup>, which is the most stable product resulting from the protonation of ketene. We have produced this species in the laboratory and observed its rotational transitions  $J_u = 10$  up to  $J_u = 27$ . Hence, we report the discovery of CH<sub>3</sub>CO<sup>+</sup> in space based on our observations, theoretical calculations, and laboratory experiments. The derived rotational and distortion constants allow us to predict the spectrum of CH<sub>3</sub>CO<sup>+</sup> with high accuracy up to 500 GHz. We derive an abundance ratio  $N(\text{H}_2\text{CCO})/N(\text{CH}_3\text{CO}^+) \sim 44$ . The high abundance of the protonated form of H<sub>2</sub>CCO is due to the high proton affinity of the neutral species. The other isomer, H<sub>2</sub>CCOH<sup>+</sup>, is found to be 178.9 kJ mol<sup>-1</sup> above CH<sub>3</sub>CO<sup>+</sup>. The observed intensity ratio between the  $K=0$  and  $K=1$  lines,  $\sim 2.2$ , strongly suggests that the *A* and *E* symmetry states have suffered interconversion processes due to collisions with H and/or H<sub>2</sub>, or during their formation through the reaction of H<sub>3</sub><sup>+</sup> with H<sub>2</sub>CCO.

Correspondence to: J. Cernicharo.

jose.cernicharo@csic.es.

★Based on observations carried out with the Yebes 40m telescope (projects 19A003, 20A014, and 20D15) and the Institut de Radioastronomie Millimétrique (IRAM) 30m telescope. The 40m radiotelescope at Yebes Observatory is operated by the Spanish Geographic Institute (IGN, Ministerio de Transportes, Movilidad y Agenda Urbana). IRAM is supported by INSU/CNRS (France), MPG (Germany), and IGN (Spain).

## Keywords

Astrochemistry; ISM: molecules; ISM: individual (TMC-1); line: identification; molecular data

---

## 1 Introduction

The cold dark core TMC-1 presents an interesting chemistry. It produces a significant number of the molecules detected in space, in particular long neutral carbon-chain radicals and their anions (see e.g. Cernicharo et al. 2020a; Marcelino et al. 2020a, and references therein) as well as cyanopolyynes (see Cernicharo et al. 2020b and Xue et al. 2020, and references therein). The presence in this object of O-bearing carbon chains, such as C<sub>2</sub>O (Ohishi et al. 1991), C<sub>3</sub>O (Matthews et al. 1984), HC<sub>5</sub>O (McGuire et al. 2017), HC<sub>7</sub>O (Cordiner et al. 2017), HCCO, and HC<sub>3</sub>O<sup>+</sup> (Cernicharo et al. 2020c), is a surprising result that has not yet been fully accounted for by chemical models.

The abundance of polyatomic cations in cold interstellar clouds is relatively low because they react fast with electrons. Interestingly, all polyatomic cations detected in cold clouds are protonated forms of stable and abundant molecules. Chemical models and observations suggest a trend in which the protonated-to-neutral abundance ratio [MH<sup>+</sup>]/[M] increases with the proton affinity of M (Agúndez et al. 2015; Cernicharo et al. 2020c,d; Marcelino et al. 2020a).

It has been suggested that some O-bearing cations are sufficiently long-lived to be abundant (Petrie et al. 1993). We have recently reported the discovery of the cation HC<sub>3</sub>O<sup>+</sup> in TMC-1 (Cernicharo et al. 2020c). In this letter, we report the detection of two series of lines that are harmonically related towards the cold dark core TMC-1. These lines can be fitted as the  $K=0$  and  $K=1$  lines of a symmetric rotor. From the astronomical data and the derived rotational constants, together with high-level *ab initio* calculations, we suggest CH<sub>3</sub>CO<sup>+</sup> as the best possible carrier. We have performed microwave laboratory experiments that fully support this hypothesis: We detected 79 rotational transitions near the predicted frequencies from the astronomical constants. Hence, we report the discovery in space and in the laboratory of CH<sub>3</sub>CO<sup>+</sup> (acetyl cation), which is the most stable isomer resulting from the protonation of ketene (H<sub>2</sub>CCO). The presence of CH<sub>3</sub>CO<sup>+</sup> can be expected on the basis of the high abundance of H<sub>2</sub>CCO in TMC-1 and its large proton affinity (825.3 kJ mol<sup>-1</sup>; Traeger et al. 1982). An anomalous abundance ratio of 2.2 is found between the *A* and *E* symmetry species of CH<sub>3</sub>CO<sup>+</sup>. We discuss these results in the context of state-of-the-art chemical models and in terms of the interconversion of *E*-CH<sub>3</sub>CO<sup>+</sup> into *A*-CH<sub>3</sub>CO<sup>+</sup> through the formation process of the molecule or by collisions with H and/or H<sub>2</sub>.

## 2 Observations

New receivers, built as part of the Nanocosmos project<sup>1</sup> and installed at the Yebes 40m radio telescope, were used for the observations of TMC-1. The Q-band receiver consists of two high electron mobility transistor (HEMT) cold amplifiers that cover the 31.0-50.3 GHz band

---

<sup>1</sup> <https://nanocosmos.iff.csic.es/>

with horizontal and vertical polarizations. Receiver temperatures vary from 22 K at 32 GHz to 42 K at 50 GHz. The spectrometers are  $2 \times 8 \times 2.5$  GHz fast Fourier transform spectrometers (FFTs) with a spectral resolution of 38.1 kHz, providing the whole coverage of the Q-band in both polarizations. The main beam efficiency varies from 0.6 at 32 GHz to 0.43 at 50 GHz (Tercero et al. 2020).

The observations that led to the line survey in the Q-band towards TMC-1 ( $\alpha_{J2000} = 4^{\text{h}}41^{\text{m}}41.9^{\text{s}}$  and  $\delta_{J2000} = +25^{\circ}41'27.0''$ ) were performed in several sessions, between November 2019 and February 2020. The observing procedure was frequency switching with a frequency throw of 10 MHz. The nominal spectral resolution of 38.1 kHz was used for the final spectra. In these runs, two different frequency coverages were observed, 31.0849.52 GHz and 31.98-50.42 GHz. This permits the user to check that no spurious ghosts are produced in the down-conversion chain, in which the signal coming from the receiver is down-converted to 1-19.5 GHz and then split into eight bands with a coverage of 2.5 GHz, each of which are analysed by the FFTs. Additional data were taken in October 2020 to improve the line survey at some frequencies and to further check the consistency of all observed spectral features. These observations were also performed in frequency switching but with a throw of 8 MHz. The sensitivity varies along the Q-band between 0.5 and 2.5 mK, which is a considerable improvement compared to previous line surveys in the 31-50 GHz frequency range (Kaifu et al. 2004).

The IRAM 30m data come from a line survey performed towards TMC-1 and B1, and the observations have been described by Marcelino et al. (2007) and Cernicharo et al. (2012). The observations of L1527 and L1544 were obtained as part of the IRAM 30m Large Program ASAI and were described by Lefloch et al. (2018). The intensity scale and antenna temperature ( $T_A^*$ ) for the two telescopes used in this work were calibrated using two absorbers at different temperatures as well as the atmospheric transmission model ATM (Cernicharo 1985; Pardo et al. 2001). Calibration uncertainties were adopted to be 10 %. All data were analysed using the GILDAS package<sup>2</sup>.

### 3 Results and discussion

The assignment of the observed features in our line surveys was done using the CDMS and JPL catalogues (Müller et al. 2005; Pickett 1998) and the MADEx code (Cernicharo 2012). Most of the weak lines found in our survey of TMC-1 can be assigned to known species and their isotopologues. Nevertheless, many features remain unidentified. Frequencies for the unknown lines were derived by assuming a local standard of rest velocity of  $5.83 \text{ km s}^{-1}$ , a value that was derived from the observed transitions of  $\text{HC}_5\text{N}$  and its isotopologues in our line survey (Cernicharo et al. 2020a,b). Our new data towards TMC-1 allowed us to detect  $\text{C}_3\text{N}^-$  and  $\text{C}_5\text{N}^-$  (Cernicharo et al. 2020a), as well as new species such as the isocyano isomer of  $\text{HC}_5\text{N}$ ,  $\text{HC}_4\text{NC}$  (Cernicharo et al. 2020b), the cation  $\text{HC}_3\text{O}^+$  (Cernicharo et al. 2020c), the cation  $\text{HC}_3\text{S}^+$  (Cernicharo et al. 2020d), and the cation  $\text{HC}_5\text{NH}^+$  (Marcelino et al. 2020a), in addition to several tens of already known molecules and their isotopologues.

<sup>2</sup> <http://www.iram.fr/IRAMFR/GILDAS>

Within the unidentified features in our surveys in the 3 mm band and the Q-band, we found two series of four lines with a harmonic relation of 2:4:5:6 (see Fig. 1). Taking into account the line density in TMC-1, the possibility that the observed pattern is fortuitous is very small. The observed lines are shown in Fig. 1, and the derived line parameters are given in Table 1. In fact, the  $J=5-4$  line at 91342 MHz has intrigued us since 2017 when we detected it in TMC-1, L483, L1527, and L1544. We interpreted the  $K=0,1$  lines and the U line at  $\sim 91344$  (see Fig. A.1) as the hyperfine structure of a  $J=1-0$  or  $J=2-1$  transition of a molecule containing a nucleus with a spin of 1. Using the old receivers of the Yebes 40 m telescope, and assuming that the three lines around 91342 MHz could correspond to  $J=2-1$ , we searched for lines at 45671 MHz without success. Only when the new receivers covering the whole Q-band were available at the telescope, and we detected the doublet at 36537 MHz (see Fig. 1), did we realize that two of the lines around 91342 MHz correspond to a  $J=5-4$  transition in harmonic relation 2:5 with the 36537 MHz doublet. Moreover, the U line at 91344 MHz is produced by another carrier as it is detected in B1, while the other lines are not. Once we relaxed the initial idea that these features were the hyperfine structure of a low- $J$  transition, other features were found in the 3 mm domain ( $J=4-3$  and  $J=6-5$ , as well as  $J=7-6$  in L1527).

The two series of lines can be fitted to two linear rotors with rotational constants  $B = 9134.4738 \pm 0.0006$  MHz and  $B = 9134.2860 \pm 0.0020$  MHz. The distortion constant is exactly the same for both series,  $D = 4.00 \pm 0.02$  kHz. The observed spectra is reminiscent of the  $K=0$  and  $K=1$  components of the rotational transitions of a symmetric rotor. In fact, the eight observed lines in TMC-1 can be fitted with a single rotational constant and two distortion constants if we assume that the carrier is the same for both series and that it has a  $C_{3v}$  symmetry (i.e. that it is a symmetric rotor). Using the standard Hamiltonian for this kind of molecular rotor (Gordy & Cook 1984), we derived the rotational and distortion constants provided in Table 2.

From the derived rotational constant, 9134 MHz, the molecule should contain at least three atoms between C, N, and O. We analysed the possible candidates that could have a rotational constant similar to the observed one. Detailed *ab initio* calculations for the possible linear and asymmetric carriers are given in Appendix B. Concerning symmetric rotors, it is amazing to realize that all  $\text{CH}_3\text{X}$ , with  $\text{X}=\text{CN}$ ,  $\text{NC}$ , and  $\text{CCH}$ , have rotational constants close to our rotational and distortion constants. For example,  $\text{CH}_3\text{CN}$  has a rotational constant of 9198.9 MHz (Müller et al. 2009), which is really very close to our result. The other possible candidates,  $\text{CH}_3\text{CNH}^+$  ( $B=8590.5$  MHz; Amano et al. 2006) and  $\text{CH}_3\text{NCH}^+$  (see, Table B.1), are too heavy. Hence, the best symmetric rotor candidate seems to be a species similar to  $\text{CH}_3\text{CN}$ . The acetyl radical,  $\text{C}_2\text{H}_3\text{O}$ , has been observed in the laboratory by Hirota et al. (2006), but it is asymmetric and its lines show a very complex hyperfine structure. However,  $\text{CH}_3\text{CO}^+$  is a symmetric rotor (Mosley et al., 2014) and the lowest energy isomer of  $\text{H}_3\text{C}_2\text{O}^+$ . Its possible precursor, if formed through protonation, is ketene, which is one of the most abundant O-bearing species in TMC-1 (see Cernicharo et al. 2020c).

### 3.1 Quantum chemical calculations and assignment to $\text{CH}_3\text{CO}^+$

Precise geometries and spectroscopic molecular parameters for the species mentioned above were computed using high-level *ab initio* calculations. The first screening for all plausible candidates (see Appendix B) was done at the CCSD/cc-pVTZ level of theory (Cížek 1969; Dunning 1989). These results are shown in Table B.1. In a second stage, the most promising candidates, namely  $\text{CH}_3\text{CO}^+$ ,  $\text{CH}_2\text{COH}^+$ , and  $\text{CH}_3\text{NCH}^+$ , were calculated at the CCSD(T)-F12b/aug-cc-pVQZ levels of theory (Raghavachari et al. 1989; Adler et al. 2007; Knizia et al. 2009). To obtain more precise values for the rotational parameters of these three species, we calibrated our calculations using experimental to theoretical scaling ratios for analogue molecular species. This method has been proved to be suitable to accurately reproduce the molecular geometry of other identified molecules (Cernicharo et al. 2019; Marcelino et al. 2020a; Cernicharo et al. 2020c). In our present case, we used  $\text{CH}_3\text{CN}$ ,  $\text{CH}_2\text{CNH}$ , and  $\text{CH}_3\text{NC}$ , which are isoelectronic species of  $\text{CH}_3\text{CO}^+$ ,  $\text{CH}_2\text{COH}^+$ , and  $\text{CH}_3\text{NCH}^+$ , respectively, for this purpose. Table B.2 shows the results of these calculations, which are summarized in Table 3. As can be seen, the employed level of theory reproduces the rotational parameters for  $\text{CH}_3\text{CN}$ ,  $\text{CH}_2\text{CNH}$ , and  $\text{CH}_3\text{NC}$  very well, with relative discrepancies around 0.08% and 0.04% for  $B$  in the cases of  $\text{CH}_3\text{CN}$  and  $\text{CH}_3\text{NC}$ , respectively. After correcting the calculated parameters for  $\text{CH}_3\text{CO}^+$ ,  $\text{CH}_2\text{COH}^+$ , and  $\text{CH}_3\text{NCH}^+$  using the derived scaling ratios for  $\text{CH}_3\text{CN}$ ,  $\text{CH}_2\text{CNH}$ , and  $\text{CH}_3\text{NC}$ , respectively, we obtained a  $B$  constant of 9129.62 MHz for  $\text{CH}_3\text{CO}^+$ , which shows the best agreement with that derived from the TMC-1 lines. The centrifugal distortion values, obtained in the same manner but at the MP2/aug-cc-pVQZ level of theory for  $\text{CH}_3\text{CO}^+$  and  $\text{CH}_3\text{NCH}^+$ , are both compatible with those obtained from the fit of the lines. The agreement between the experimental constants and those calculated for  $\text{CH}_2\text{COH}^+$  is substantially worse. The calculated dipole moments for  $\text{CH}_3\text{CO}^+$  and  $\text{CH}_3\text{NCH}^+$  are 3.5 D and 2.0 D, respectively, while the  $\mu_a$  and  $\mu_b$  values for  $\text{CH}_2\text{COH}^+$  are 0.8 and 1.7 D, respectively.

In addition to the geometry optimizations, we calculated the energy associated with the plausible formation of  $\text{CH}_3\text{CO}^+$ , starting from ketene and three proton donors;  $\text{H}_3^+$ ,  $\text{H}_3\text{O}^+$ , and  $\text{HCO}^+$ . All these calculations were carried out at the CCSD/cc-pVTZ level of theory. We found a total energy change in the protonation of ketene to form  $\text{CH}_3\text{CO}^+$  of  $-421.8$ ,  $-130.9$ , and  $-244.8$  kJ mol $^{-1}$  when ketene reacts with  $\text{H}_3^+$ ,  $\text{H}_3\text{O}^+$ , and  $\text{HCO}^+$ , respectively. More details can be found in Appendix C.

### 3.2 Laboratory detection of $\text{CH}_3\text{CO}^+$

We conducted an experiment to detect the  $\text{CH}_3\text{CO}^+$  cation in the laboratory using rotational spectroscopy below 500 GHz. The experimental setup was similar to the one used to detect  $\text{NS}^+$  (Cernicharo et al. 2018). The cation was produced in a liquid-nitrogen-cooled Pyrex absorption cell by glow-discharging a mixture of  $\text{CH}_4$ ,  $\text{CO}$  (1:1), and Ar. A solenoid coil wound on the cell can generate an axial magnetic field (up to 300 G) to magnetically extend the negative glow, the region known to produce the highest concentrations of cations (compared to the positive column discharge; De Lucia et al. 1983). We also tried acetone and acetaldehyde as precursors (Mosley et al., 2014), but without success.

To optimize the experimental setup, we first observed the  $J=2\leftarrow 1$  transition of  $\text{HCO}^+$  at 178375.056 MHz, which was produced in the same gas mixture. We then searched for the  $J=10\leftarrow 9$ ,  $K=0-2$  series of lines of  $\text{CH}_3\text{CO}^+$  between 182.658 and 182.675 GHz based on the rotational constants derived from the lines observed in TMC-1. Weak spectra were observed within 500 kHz. The best experimental conditions were found to be  $P(\text{CH}_4)=P(\text{CO})=1.5$  mTorr,  $P(\text{Ar})=5.5$  mTorr (gas mixture cooled using liquid nitrogen but pressures measured at room temperature), an electric discharge of 3.5 kV/10 mA, and an axial magnetic field of 200 G. These lines disappeared when one of the precursors was suppressed, or when the axial magnetic field was cut off. The latter phenomenon confirmed almost unambiguously that they were due to a cation. Subsequent measurements of higher- $J$  transitions fully support the astrophysical assignment of the observed lines to  $\text{CH}_3\text{CO}^+$ .

In total, 79 lines were observed in the laboratory with quantum numbers in the ranges  $J=10-27$  and  $K \leq 6$  (see Table E.1). Transitions occurring below 330 GHz were measured by standard frequency modulation absorption spectroscopy, resulting in second-derivative lineshapes. These lines ( $K \leq 3$ ) were found unshifted from the first prediction. Those from 400 to 500 GHz were measured by emission spectroscopy (Zou et al. 2020), giving Voigt-profile lineshapes. Compared to the prediction, some deviations were observed up to 1 MHz for  $K=6$ ; these measurements led us to determine the  $H_{JK}$  and  $H_{KJ}$  centrifugal distortion terms. For maximum sensitivity, these lines were measured using the single frequency excitation method with 5-20 million acquisitions (which took 1 to 5 min.). Additionally, a 120 MHz wide chirped excitation spectrum, measured with 67 million acquisitions, is given in Fig. 2 for illustration and comparison purposes. The uncertainty of the laboratory frequency measurements are estimated to be 50 kHz. Given the mass of the cation, and that the negative glow is a nearly electric field-free region, the reported laboratory frequencies are expected to be unshifted by the Doppler effect. The separate and merged least-squares analysis of all (astronomical and laboratory) measured transitions are provided in Table 2. The measured frequencies and the observed minus calculated values are given in Table E.1. Frequency predictions are given in Table E.2.

### 3.3 Chemistry of $\text{CH}_3\text{CO}^+$

From the observed line intensities of  $\text{CH}_3\text{CO}^+$ , we derived a rotational temperature of  $\sim 5$  K and a total column density of  $(3.2 \pm 0.3) \times 10^{11} \text{ cm}^{-2}$  (see Appendix D). The column densities for the  $A$  and  $E$  species are  $(2.2 \pm 0.2) \times 10^{11} \text{ cm}^{-2}$  and  $(9.7 \pm 0.9) \times 10^{10} \text{ cm}^{-2}$ , respectively. Adopting the column density for ketene derived by Cernicharo et al. (2020c), we obtained a  $\text{H}_2\text{CCO}/\text{CH}_3\text{CO}^+$  ratio of 44. Assuming the  $\text{H}_2$  column density derived by Cernicharo & Guélin (1987), the abundance of  $\text{CH}_3\text{CO}^+$  is  $3.2 \times 10^{-11}$ .

The chemistry of protonated molecules in cold dense clouds has been discussed by Agúndez et al. (2015). Chemical model calculations similar to those that they presented predict that the abundance of protonated ketene is controlled by the typical routes operating for protonated molecules. That is,  $\text{CH}_3\text{CO}^+$  is mostly formed by proton transfer to  $\text{H}_2\text{CCO}$  from  $\text{HCO}^+$ ,  $\text{H}_3^+$ , and  $\text{H}_3\text{O}^+$ , while it is destroyed through dissociative recombination with electrons. The radiative association between  $\text{CH}_3^+$  and CO is also an important route to  $\text{CH}_3\text{CO}^+$ . The abundance ratio  $\text{H}_2\text{CCO}/\text{CH}_3\text{CO}^+$  predicted by the model is in the range

250–450 and depends on whether the UMIST RATE12 (McElroy et al. 2013) or KIDA `kida.uva.2014` (Wakelam et al. 2015) chemical networks are used. As occurs for most protonated molecules observed in cold dense clouds, the abundance of the protonated form with respect to the neutral is underestimated by the chemical model. In this case, there is a factor of 5–10 difference between the model and observations. Incorrect estimates for the rate constants of the dominant reactions of the formation and destruction of  $\text{CH}_3\text{CO}^+$  may be behind this disagreement. Alternatively, the chemical network may miss some important formation route to  $\text{CH}_3\text{CO}^+$ , although it is difficult to identify reactions producing this ion from abundant reagents. For example, plausible reactions of  $\text{CH}_n^+$  ions with  $\text{CO}$ ,  $\text{H}_2\text{CO}$ , or  $\text{CH}_3\text{OH}$  tend to form products other than  $\text{CH}_3\text{CO}^+$  (Adams & Smith 1978). In this context, it is worth noting that not all species resulting from the protonation of abundant molecules in TMC-1 are detected. For example,  $\text{CH}_3\text{CNH}^+$  is not detected in TMC-1 despite the  $\text{CH}_3\text{CN}$  proton affinity of  $787.4 \pm 5.9 \text{ kJ mol}^{-1}$  (Williams et al. 2001). The  $3\sigma$  upper limit to the column density of  $\text{CH}_3\text{CNH}^+$  is  $2.5 \times 10^{11} \text{ cm}^{-2}$ . The column density of  $\text{CH}_3\text{CN}$  is  $(3.2 \pm 0.2) \times 10^{12} \text{ cm}^{-2}$  (see Appendix A); hence, the abundance ratio between the neutral and its protonated form is 13. The low dipole moment of  $\text{CH}_3\text{CNH}^+$  compared to that of  $\text{CH}_3\text{CN}$  (1.01 D versus 3.93 D) limits the chances of detecting this species.

### 3.4 A- $\text{CH}_3\text{CO}^+$ /E- $\text{CH}_3\text{CO}^+$ abundance ratio

The column densities derived for the *A* and *E* species of  $\text{CH}_3\text{CO}^+$  are not identical, as would be expected for a symmetric top. The *A/E* abundance ratio for this molecule is 2.27. However, all symmetric molecules of  $\text{CH}_3\text{X}$  detected in TMC-1 have an abundance ratio between their *A* and *E* species that is close to unity (see Appendix D and Fig. D.2). In a symmetric top, the two symmetry states *A* and *E* are not connected radiatively nor through inelastic collisions with  $\text{H}_2$ . Unlike the rest of the  $\text{CH}_3\text{X}$  molecules detected in TMC-1,  $\text{CH}_3\text{CO}^+$  is a cation, and its reactive collisions with  $\text{H}_2$  or  $\text{H}$  could produce a proton interchange if there is no barrier to the reaction. The lowest energy level of the *E* symmetry state is the  $J=1$ ,  $K=1$ , which is 7.8 K above the ground  $J=0$ ,  $K=0$  level of the *A* state. Hence, the reaction of interchange of a proton  $E\text{-CH}_3\text{CO}^+ + \text{H}_2/\text{H} \rightarrow A\text{-CH}_3\text{CO}^+ + \text{H}_2/\text{H} + 7.8 \text{ K}$  is exothermic, although it is unknown if there is a barrier; this is something that has to be established via detailed theoretical calculations. At thermal equilibrium, and for a kinetic temperature of 10 K, the *A/E* abundance ratio could be  $e^{0.78} = 2.18$ , which is very close to the observed value of 2.27. For neutral molecules with two or more symmetric hydrogens, the proton interchange could be mainly produced through collisions with  $\text{H}^+$ ,  $\text{H}_3^+$ ,  $\text{HCO}^+$ , and  $\text{H}_3\text{O}^+$ , which are much less abundant than  $\text{H}_2$  and  $\text{H}$ . In Appendix D, we discuss the *A/E* abundance ratio of all neutral symmetric rotors that have been detected so far in TMC-1, including  $\text{CH}_3\text{NC}$ , which has previously only been observed in two cold dense clouds: L1544 (Jiménez-Serra et al. 2016) and L483 (Agúndez et al. 2019). For all these species, the *A/E* abundance ratio is close to unity.

Alternatively, we could also consider the possibility that the collisional rates of the acetyl cation with  $\text{H}_2$  or  $\text{He}$  are higher for the *A* species than for the *E* species. As the acetyl cation is isoelectronic to  $\text{CH}_3\text{CN}$ , we could use the collisional rates of the latter species (Khalifa et al. 2020) to estimate possible differences in the excitation temperature of the  $K=0$  and  $K=1$  lines. We explored a density range of  $(4 - 10) \times 10^4 \text{ cm}^{-3}$  and a kinetic temperature range of

5-10 K. No significant differences were found in the predicted brightness temperature between these lines. Of course, if the effect is due to inelastic collisions, then methyl cyanide ( $\text{CH}_3\text{CN}$ ) would also show a similar behaviour. Nevertheless, although both species are isoelectronic, the fact that  $\text{CH}_3\text{CO}^+$  is positively charged could result in very different collisional rates with  $\text{H}_2$  compared to  $\text{CH}_3\text{CN}$ .

We could also consider that the  $A/E$  abundance ratio is affected by the formation process of the molecule. As shown in Sect. 3.1, the reaction of ketene with  $\text{H}_3^+$  is the most favourable for protonation from the thermodynamical point of view. Both species, ketene and  $\text{H}_3^+$ , could also have their ortho/para ratio affected by the low temperature of dense dark clouds, which will introduce a non-trivial spin statistic into the formation process of  $\text{CH}_3\text{CO}^+$ . Additional calculations are needed to evaluate the role of collisional excitation and of spin interchange in order to understand the anomalous behaviour exhibited by the  $A$  and  $E$  symmetry species of  $\text{CH}_3\text{CO}^+$ .

## Supplementary Material

Refer to Web version on PubMed Central for supplementary material.

## Acknowledgements

The Spanish authors thank Ministerio de Ciencia e Innovación for funding support through project AYA2016-75066-C2-1-P, PID2019-106235GB-I00 and PID2019-107115GB-C21 / AEI / 10.13039/501100011033. We also thank ERC for funding through grant ERC-2013-Syg-610256-NANOCOSMOS. MA and CB thanks Ministerio de Ciencia e Innovación for grants RyC-2014-16277 and FJCI-2016-27983, respectively. Y. Endo thanks Ministry of Science and Technology of Taiwan through grant MOST108-2113-M-009-25. We would like to thank Evelynne Roueff and Octavio Roncero for useful comments and suggestions.

## References

- Adams NG, Smith D. *Chem Phys Lett.* 1978; 54:530.
- Adler TB, Knizia G, Werner H-J. *J Chem Phys.* 2007; 127
- Agúndez M, Cernicharo J, de Vicente P, et al. *A&A.* 2015; 579
- Agúndez M, Marcelino N, Cernicharo J, et al. *A&A.* 2019; 625
- Amano T, Hashimoto K, Hirao T. *J Mol Struct.* 2006; 795:190.
- Cernicharo, J. Internal IRAM report. IRAM; Granada: 1985.
- Cernicharo J, Guélin M. *A&A.* 1987; 176:299.
- Cernicharo, J. In: Stehl, C; Joblin, C; d'Hendecourt, L, editors. ECLA 2011: Proc of the European Conference on Laboratory Astrophysics, EAS Publications Series; Cambridge: Cambridge Univ. Press; 2012. 2012 [https://nanocosmos.iff.csic.es/?page\\_id=1619](https://nanocosmos.iff.csic.es/?page_id=1619)
- Cernicharo J, Marcelino N, Rouef E, et al. *ApJ.* 2012; 759
- Cernicharo J, Lefloch B, Agúndez M, et al. *ApJ.* 2018; 854
- Cernicharo J, Cabezas C, Pardo JR, et al. *A&A.* 2019; 630
- Cernicharo J, Marcelino N, Pardo JR, et al. *A&A.* 2020a; 641
- Cernicharo J, Marcelino N, Agúndez M, et al. *A&A.* 2020b; 642
- Cernicharo J, Marcelino N, Agúndez M, et al. *A&A.* 2020c; 642
- Cernicharo J, Cabezas C, Endo Y, et al. *A&A.* 2020d
- Cížek, J. "Advances in Chemical Physics". Hariharan, PC, editor. Vol. 14. Wiley Interscience; New York: 1969. 35
- Cordiner MA, Chamley SB, Kisiel Z, et al. *ApJ.* 2017; 850:187.



- De Lucia FC, Herbst E, Plummer GM, Blake GA. *J Chem Phys.* 1983; 78:2312.
- Dunning TH. *J Chem Phys.* 1989; 90:1007.
- Fossé D, Cernicharo J, Gerin M, Cox P. *ApJ.* 2001; 552:168.
- Gordy, W, Cook, RL. *Microwave Molecular Spectra, Chapter V.* Wiley; New York: 1984.
- Hirota E, Mizoguchi A, Ohshima Y, et al. *Mol Phys.* 2006; 105:455.
- Jiménez-Serra I, Vasyunin AI, Caselli P, et al. *ApJ.* 2016; 830
- Kaifu N, Ohishi M, Kawaguchi K, et al. *PASJ.* 2004; 56:69.
- Khalifa MB, Quintas-Sánchez E, Dawes R, et al. *PCCP.* 2020; 22
- Knizia G, Adler TB, Werner H-J. *J Chem Phys.* 2009; 130
- Latanzi V, Thorwirth S, Gottlieb C, McCarthy MC. *J Phys Chem Lett.* 2012; 3:3420. [PubMed: 26290966]
- Lefloch B, Bachiller R, Ceccarelli C, et al. *MNRAS.* 2018; 477:4792.
- Marcelino N, Cernicharo J, Agúndez M, et al. *ApJ.* 2007; 665
- Marcelino N, Cernicharo J, Tercero B, et al. *ApJ.* 2009; 690
- Marcelino N, Brünken S, Cernicharo J, et al. *A&A.* 2010; 516
- Marcelino N, Agúndez M, Tercero B, et al. *A&A.* 2020a; 643
- Marcelino N, Tercero B, Agúndez M, Cernicharo J. *A&A.* 2020b
- McElroy D, Walsh C, Markwick AJ, et al. *A&A.* 2013; 550
- McGuire BA, Burkhardt M, Shingledecker CN, et al. *ApJ.* 2017; 843
- Matthews HE, Irvine E, Friberg FM, et al. *Nature.* 1984; 310:125. [PubMed: 11541993]
- Mosley JD, Young JW, Duncan MA. *J Chem Phys.* 2014; 141
- Müller HSP, Schlöder F, Stutzki J, Winnewisser G. *J Mol Struct.* 2005; 742:215.
- Müller HSP, Drouin BJ, Pearson JC. *A&A.* 2009; 506:1487.
- Müller HSP, Maeda A, Thorwirth S, et al. *A&A.* 2019; 621
- Neill JL, Muckle MT, Zaleski DP, et al. *ApJ.* 2012; 755:153.
- Ohishi M, Suzuki H, Ishikawa S-I, et al. *ApJ.* 1991; 380
- Rodler M, Brown RD, Godfrey PD, Tack LM. *Chem Phys Lett.* 1984; 110:447.
- Pardo JR, Cernicharo J, Serabyn E. *IEEE Trans Antennas and Propagation.* 2001; 49:12.
- Petrie S, Bettens RPA, Freeman CG, McEwan MJ. *MNRAS.* 1993; 264:862.
- Pickett HM, Boyd TL. *J Mol Spectrosc.* 1979; 75:53.
- Pickett HM, Poynter RL, Cohen EA, et al. *J Quant Spectrosc Radiat Transfer.* 1998; 60:883.
- Plíva J, Le LD, Johns JWC, et al. *J Mol Spectrosc.* 1995; 173:423.
- Raghavachari K, Trucks GW, Pople JA, Head-Gordon M. *Chem Phys Lett.* 1989; 157:479.
- Sakai N, Sakai T, Hirota T, Yamamoto S. *ApJ.* 2009; 702:1025.
- Tercero B, Pardo JR, Cernicharo J, Goicoechea J. *A&A.* 2010; 517
- Tercero B, Vincent L, Cernicharo J, et al. *A&A.* 2011; 528
- Tercero F, López-Pérez JA, Gallego, et al. *A&A.* 2020; 645
- Traeger JC, McLoughlin RG, Nicholson AJC. *J Am Chem Soc.* 1982; 104:5318.
- Vastel C, Yamamoto S, Lefloch B, Bachiller R. *A&A.* 2015; 582
- Wakelam V, Loison J-C, Herbst E, et al. *ApJS.* 2015; 217:20.
- Williams TI, Denault JW, Cooks RG. *Int J Mass Spectrom.* 2001; 210:133.
- Xue C, Willis ER, Loomis RA, et al. *ApJ.* 2020; 900
- Zou L, Motiyenko RA, Margulès L, Alekseev A. *Review of Scientific Instruments.* 2020; 91

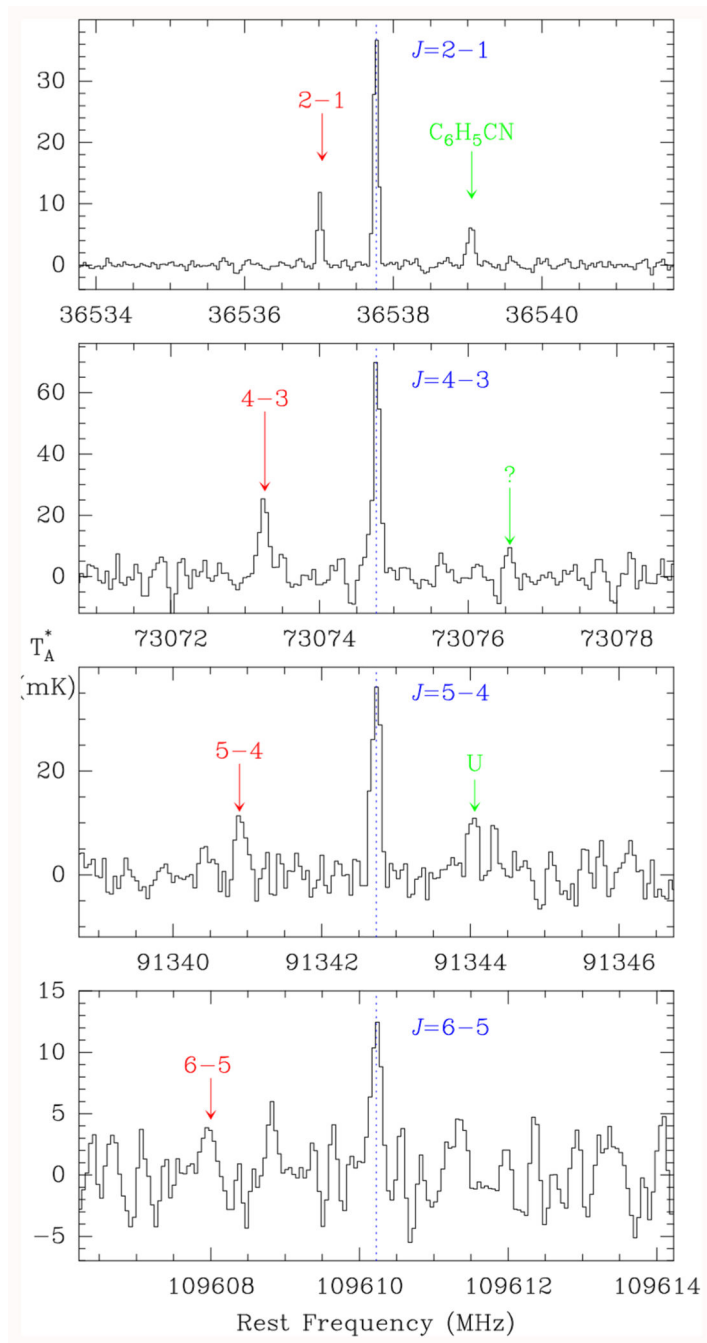


**Fig. 1.** Observed lines of  $\text{CH}_3\text{CO}^+$  towards TMC-1. The abscissa corresponds to rest frequencies (in MHz) assuming a local standard of rest velocity of  $5.83 \text{ km s}^{-1}$  (Cernicharo et al. 2020a,b). Frequencies and intensities for the observed lines are given in Table 1. The ordinate is the antenna temperature (in mK). Spectral resolution is  $38.1 \text{ kHz}$  below  $50 \text{ GHz}$  and  $48.8 \text{ kHz}$  above. The blue labels correspond to the series of lines we assign to the  $A$  species of  $\text{CH}_3\text{CO}^+$ , while the red ones correspond to those of the  $E$  species.

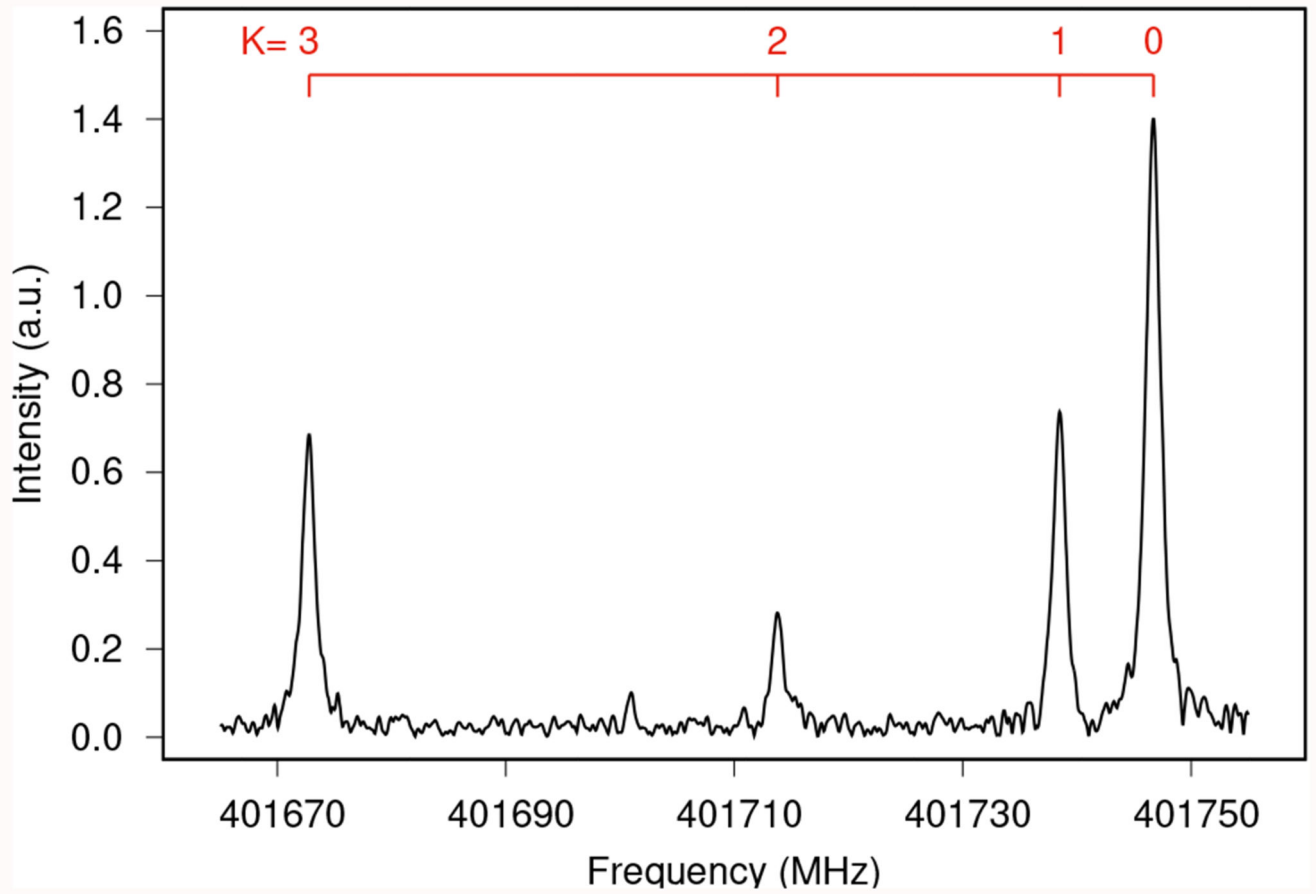


**Fig. 2.**  $J=22 \rightarrow 21$ ,  $K=0-3$  transitions obtained by chirped-pulsed excitation. The record corresponds to the average of 67 million spectra acquired in  $\sim 20$  min.

**Table 1**  
**Observed line parameters for CH<sub>3</sub>CO<sup>+</sup> in TMC-1.**

$J_u$	$K$	$\nu_{obs}^a$ (MHz)	$\Delta\nu_{oc}^b$ (kHz)	$T_A^*{}^c$ (mK)	$\nu^d$ (kms <sup>-1</sup> )	$\int T_A^* dv^e$ (mK km s <sup>-1</sup> )
2	0	36537.765	-3.5	39.0±0.6	0.63±0.01	26.1±0.6
2	1	36537.014	-0.6	11.8±0.6	0.60±0.03	7.5±0.6
4	0	73074.769	2.7	71.0±3.5	0.47±0.03	35.7±2.0
4	1	73073.252	-6.6	25.0±3.5	0.65±0.11	17.2±2.0
5	0	91342.732	-3.5	37.5±3.0	0.46±0.04	18.2±1.0
5	1	91340.865	14.2	11.9±3.0	0.49±0.11	6.3±1.0
6	0	109610.225	2.1	12.8±2.8	0.45±0.09	6.1±1.0
6	1	109607.954	-7.3	6.6±2.8	0.60±0.10	4.2±1.0

**Notes.**

<sup>a</sup> Observed frequencies (in MHz) adopting a  $v_{LSR}$  of 5.83 km s<sup>-1</sup> for TMC-1. The uncertainty is 10 kHz for all the lines.

<sup>b</sup> Observed minus calculated frequencies (in kHz) resulting from a fit to the observed frequencies. The  $J=7-6$   $K=0,1$  lines observed in L1527 have been included in the fit (see text).

<sup>c</sup> Antenna temperature (in mK).

<sup>d</sup> Linewidth at half intensity (in kms<sup>-1</sup>). (<sup>e</sup>) Integrated line intensity (in mKkms<sup>-1</sup>).

**Table 2**  
**Derived spectroscopic parameters (in MHz) for CH<sub>3</sub>CO<sup>+</sup>.**

Constant	Space <sup>a</sup>	Laboratory <sup>b</sup>	Merged <sup>c</sup>
$B$	9134.47424(82)	9134.47083(27)	9134.47211(20)
$D_J$	$4.014(12) 10^{-3}$	$3.99198(25) 10^{-3}$	$3.99307(21) 10^{-3}$
$D_{JK}$	$1.8847(53)10^{-1}$	$1.87616(41) 10^{-1}$	$1.87736(46) 10^{-1}$
$H_{JK}$		$8.66(33) 10^{-7}$	$9.56(37) 10^{-7}$
$H_{KJ}$		$6.58(59) 10^{-6}$	$7.19(74) 10^{-6}$
$rms(kHz)^d$	6.9	34.3	33.2
$J_{min}/J_{max}$	1/7	10/27	1 /27
$K_{min}/K_{max}$	0/1	0/6	0/6
$N_{lines}^e$	10	79	89
$\nu_{max}(GHz)$	127.87	492.95	492.95

**Notes.**

<sup>a</sup>Fit to the lines of CH<sub>3</sub>CO<sup>+</sup> observed in TMC-1. In this fit, the  $J=7-6$  and  $K=0,1$  lines observed in L1527 (with frequencies of  $127877.133\pm 0.025$  and  $127874.494\pm 0.050$  MHz, respectively) have been included (see Fig. A.1 and Appendix A).

<sup>b</sup>Fit to the lines of CH<sub>3</sub>CO<sup>+</sup> observed in the laboratory.

<sup>c</sup>Fit to the the lines of CH<sub>3</sub>CO<sup>+</sup> observed in space and in the laboratory.

<sup>d</sup>The standard deviation of the fit (in kHz). (<sup>e</sup>) Number of lines included in the fit.

**Table 3**  
**Scaled theoretical values for the spectroscopic parameters of  $\text{CH}_3\text{CO}^+$ ,  $\text{CH}_2\text{COH}^+$ , and  $\text{CH}_3\text{NCH}^+$  together with the experimental values obtained in this work (all in MHz).**

Parameter	Exp. <sup>a</sup>	$\text{CH}_3\text{CO}^+$	$\text{CH}_2\text{COH}^+$	$\text{CH}_3\text{NCH}^+$
$B$	9134.4742(8)	9129.6	9309.5 <sup>b</sup>	9105.5
$D_J \times 10^{-3}$	4.014(13)	3.9	2.8	4.0
$D_{JK} \times 10^{-3}$	188.47(50)	184.6	378.7	171.7

**Notes.**

<sup>a</sup>This work.

<sup>b</sup> $(B+C)/2$